Relaxation dynamics of bimodally distributed CdSe quantum dots

P. Bajracharya, T. A. Nguyen, S. Mackowski,* L. M. Smith, and H. P. Wagner
Department of Physics, University of Cincinnati, Cincinnati, Ohio 45221-0011, USA

U. W. Pohl and D. Bimberg
Institut für Festkörperphysik, TU Berlin, 10623 Berlin, Germany

M. Strassburg
Department of Physics and Astronomy, Georgia State University, Atlanta, Georgia 30302-4106, USA
(Received 22 February 2005; revised manuscript received 3 October 2006; published 12 January 2007)

We study the dynamical behavior of excitons in a bimodal distribution of CdSe/ZnSSe quantum dots by intensity dependent, temperature dependent, and time resolved photoluminescence. The effect of exciton localization is investigated, both experimentally and theoretically by identifying transfer mechanisms due to thermalization and redistribution of excitons. We observe a dominant exciton emission from high energy dots (QDs1) and weaker emission from low energy dots (QDs2) at 10 K and at low excitation levels. At high excitation densities a CdSe QD-precursor state becomes visible at the high energy side of the QDs1 emission. Temperature dependent photoluminescence studies reveal a thermally activated exciton transfer from QDs1 to QDs2 resulting in an enhanced QDs2 emission above 60 K. Time resolved photoluminescence measurements allow us to estimate the characteristic radiative and nonradiative decay rates as well as the trapping rate from the QD-precursor layer. The experimentally observed photoluminescence is reasonably reproduced using a coupled rate equation model.

DOI: 10.1103/PhysRevB.75.035321 PACS number(s): 73.21.La, 73.63.Kv

I. INTRODUCTION

Semiconductor quantum dot (QD) structures are of great interest due to the fundamental science and potential for novel optoelectronic devices[1–3] such as quantum dot lasers. II-VI quantum structures such as CdSe/Zn(S,Se), which have a large range of energy gaps, received considerable attention due to the tuning ability of their emission from the visible to the ultraviolet spectral range. The rapid progress in growth and characterization of self-organized QD structures leads to improved device features such as low lasing thresholds[4–10] and high characteristic temperatures.

CdSe/Zn(S,Se) QDs usually grow in a monomodal size distribution when less than 2.1 monolayers are deposited.[11–13] Despite that, such structures mostly exhibit zero-dimensional localization sites with an exponential distribution of energy states.[14] Increased mobility of charge carriers at room temperature in QD structures is assigned to redistribution, e.g., by lateral transfer between zero-dimensional localization sites.[15–18] This is one of the reasons preventing commercial application of green CdSe/(Zn,Cd)(S,Se) based laser diodes. However, no alternative material system has succeeded in the green spectral range yet. More promising have been InGaN-based laser diodes. Here, the seeming barriers to extend the emission range towards the green are attributed to the solubility gap and the presence of piezoelectric fields in ternary and quaternary group III nitride materials.[19,20]

Thermalization and redistribution of carriers strongly affect the localization properties of QDs, such as in CdSe QDs structures, where different transfer mechanisms have been identified and described experimentally and theoretically.[14–18,21] While nanocrystal QDs transfer excitation through dipole-dipole interdot interactions, Förster theory modeling shows an energy compensation only of several tens of meV.[22] On the other hand electron-phonon interactions have been found to achieve much larger energy transfer in semiconductor QDs.[23–25] In contrast resonant and nonresonant tunnel processes have been suggested to increase the carrier mobility in QD structures.[26–31] The transfer processes in semiconductor CdSe QDs are usually characterized by their direction: from initial state at higher energies to final states at lower energies. Hence, the transfer can be also described in terms of percolation of carriers and excitons as has been suggested in some reports.[16,32–34] In a more recent publication thermally activated repopulation of CdSe QD states has been also included.[35]

In this paper we report on the relaxation dynamics of excitons in CdSe/ZnSSe QD structures with a bimodal QD distribution. The two QD ensembles differ in their radiative and nonradiative excitonic lifetimes. Thermally activated redistribution of excitons in the two different sets of QDs favoring either one or the other ensemble of QDs is observed experimentally. A coupled differential equation model is developed and successfully applied to explain the unusual photoluminescence (PL) behavior. Thermal activation and phonon-assisted tunneling is proposed to facilitate carrier transfer between the QD ensembles.

II. EXPERIMENTAL DETAILS

The sample studied here was grown by metalorganic vapor phase epitaxy on (001) oriented GaAs substrate and a 5 nm thick ZnSe buffer, using DMZn-TEN, DMCd, DTBSe, and TBSH sources in 100 mbar hydrogen ambient. The quantum dot structure consists of a single CdSe layer with

1.7 monolayer nominal thickness, sandwiched between a lower and an upper lattice-matched $ZnS_{0.06}Se_{0.94}$ barrier of 70 nm and 25 nm thickness, respectively. Details of growth and sample characterization are given in Refs. 13, 36, and 37. In contrast to previous QD samples, the specific structure studied here was grown at 380 °C instead of the usually applied 350 °C. Samples prepared at this temperature show a bimodal distribution in PL spectra under the employed growth conditions. The feature is particularly pronounced, if a growth interruption of 5 s is applied after CdSe deposition and prior to ZnSSe capping. For samples grown at higher or at lower temperatures no such bimodal behavior was found. Plane-view transmission electron micrographs of the studied sample show a high QD density of $\sim 10^{11}$ cm^{-2}. In addition, defects connected to dislocations are found with a density of 8×10^8 cm^{-2}. They are supposed to originate at highly strained CdSe-rich regions.

Microphotoluminescence (μ-PL) measurements were performed at 8 K using an optical microscope objective and a cw Ar-ion laser with 476 nm excitation wavelength. The excitation intensity at the sample surface was about 1.2 W cm^{-2} at 1.7 μm spot diameter. The μ-PL signal was spectrally resolved using a diffraction grating monochromator and detected by a nitrogen cooled charged coupled device (CCD).

For temperature- and intensity-dependent PL measurements, a frequency doubled mode-locked Ti:Sapphire laser providing 100 fs pulses at a repetition rate of 80 MHz was used. The fundamental pulse emission at 870 nm was frequency doubled with a barium borate crystal in order to excite carriers within the ZnSSe barriers. The focus diameter on the sample was about 1 mm. The sample was kept in a temperature variable helium flow cryostat to enable temperature dependent measurements between 10 and 300 K. Variable neutral density filters were used to tune the incident excitation density. The PL signal was spectrally resolved and detected by the combination of a diffraction grating monochromator and a GaAs photomultiplier tube (PMT) operating in the photon counting mode.

Time resolved PL measurements were performed using a Ti:Sapphire laser producing 200 fs pulses at a wavelength of 400 nm with a repetition rate of 250 kHz. The spectrally resolved PL traces were detected by a triple diffraction grating monochromator equipped with a fast photomultiplier tube (PMT) using the time-correlated photon counting technique. The time resolution in these measurements is better than 80 ps. The sample was mounted in a variable temperature He flow cryostat that allows measurements between 10 and 130 K.

III. EXPERIMENTAL RESULTS

Figure 1 shows a typical micro-PL spectrum at 8 K on the investigated sample. The spectrum, similar to those of other quantum dot (QD) systems,[38–40] reveals ultranarrow emission lines ($\sim$0.1 meV linewidth), which we attribute to excitonic recombination in single quantum dots. Importantly, in the specific sample studied here one can decompose the asymmetric micro-PL spectrum into two broad Gaussian line shapes shown in Fig. 1 by solid and dashed lines. Since each of these bands feature identifiable single dot emission lines (see Fig. 1), we attribute them to the existence of two spectrally separated subensembles of CdSe QDs. The maximum energies of these two QD distributions are 2.602 and 2.565 eV with line widths of $\sim$30 and $\sim$60 meV, respectively. The spectral width of these lines is due to the inhomogeneous distribution of sizes, shapes, and chemical composition within each QD subset. The strong blueshift of the QD emission compared to the 1.75 eV band gap of bulk zinc blende CdSe is explained by confinement, and segregation effects as discussed in Refs. 38 and 41–44. The different confinement in the two subsets is caused by different QD size and/or different Cd concentration within the QDs.

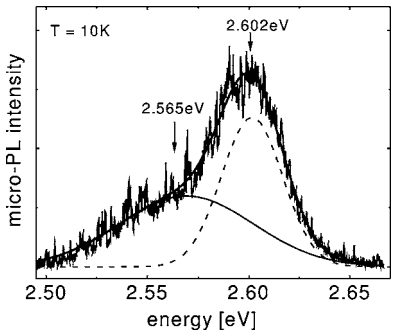

FIG. 1. Micro-PL spectrum with 1.7 μm resolution of the CdSe quantum island sample at 8 K excited with $\lambda = 476$ nm. The dashed and solid line curves show a decomposition of the spectrum into two Gaussian emission band centered at 2.602 eV and 2.565 eV.

While in previous studies the carrier redistribution has been mainly probed with a single QD ensemble (e.g., Refs. 21 and 45–48) only a few investigations have been performed in bimodal QD distributions[28,31,49–52] or quasibimodal QD distribution without a transfer from high to low energy states.[18,53] For simplicity, in what follows, the high energy and the low energy emissions are referred to as high energy dots (QDs1) and low energy dots (QDs2), respectively.

To study the carrier dynamics in this bimodal QD distribution we performed continuous wave excitation and temperature dependent macro-PL measurements. Figure 2 shows macro-PL spectra obtained at 10 K at excitation intensities ranging from 24 mW cm^{-2} to 8 W cm^{-2}. We observe a perfect correspondence between the results of macro-PL and the micro-PL experiments. As shown in Fig. 2 the QDs1 band at 2.602 eV dominates the weaker QDs2 band at 2.565 eV at low excitation intensities ($<$0.5 W cm^{-2}). The PL intensity ratio between the bands reflects the density ratio of the bimodal QD size distribution. While the total PL intensity linearly increases up to 0.8 W cm^{-2} the spectral shape and peak positions of both QD bands remain unaltered indicating no significant saturation effects within this intensity range. We believe that in this excitation intensity range the optical response is determined by excitonic recombination in CdSe QDs.

Above this excitation level the PL signal of both QD distributions broadens and the peak energies shift to lower energies. In addition a broad band appears at the high energy

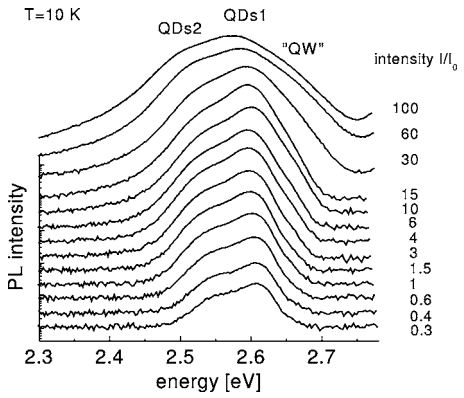

FIG. 2. Intensity dependent PL spectra at 10 K excited with 100 fs pulses at 2.85 eV. The excitation intensity is given as a ratio I/I_0 with reference intensity I_0=0.08 W cm^{-2}. QDs1 and QDs2 denote subensembles of high and low energy quantum dots, respectively, symbol QW denotes quantum well-like QD precursors of CdSe.

side of the QDs1 emission that is predominantly attributed to the quantum well-like emission (QW) arising from the CdSe QD-precursor states within the ZnSCdSe wetting layer.[54] The broadening on the high energy sides of both QD subsets is mainly due to excited QD state PL. In addition the LO-phonon sideband of the QDs1 emission may contribute to the high energy broadening of the QDs2 emission. However, since the energy distance between the PL maxima of QDs1 and QDs2 is larger than 35 meV (which increases with increasing excitation density) a dominating contribution of the QDs1 LO-phonon sideband with phonon energy ~27 meV can be excluded. The energy redshift of both QDs subsets is attributed to an increased scattering rate between excitons and weakly localized QW-like CdSe QD-precursor states and/or with free charge carriers. These scattering processes predominantly affect weakly localized QDs within each QDs subset leading to a reduced photon emission on the high-energy side of the PL bands. In addition the formation of biexcitons and negatively charged excitons shifts the center emission of both QD subsets to lower energy and gives rise to broadening on the low energy side of the PL bands.[21,43,45,55–57]

We further investigated the temperature dependence of the PL emission of the bimodal QD distribution. Such measurements provide important information about thermally induced carrier escape and subsequent recapture by strongly localized QD potentials. In order to avoid the high density effects described above, all measurements were performed at low excitation density of 0.08 W cm^{-2}. Figure 3 shows the PL spectra at temperatures ranging from 10 to 230 K. The data reveal a significant change of the spectral shapes and relative intensities between both bands ascribed to QD emission. At 10 K in addition to the dominant QDs1 and weaker QDs2 bands, we observe a very weak "QW" emission at 2.635 eV, which disappears around 40 K. When the temperature exceeds 70 K the peak energy position of both QD distributions shift towards lower energy and the intensity of the QDs1 peak rapidly decreases, whereas the QDs2 peak almost retains its intensity. At temperatures between 90 K

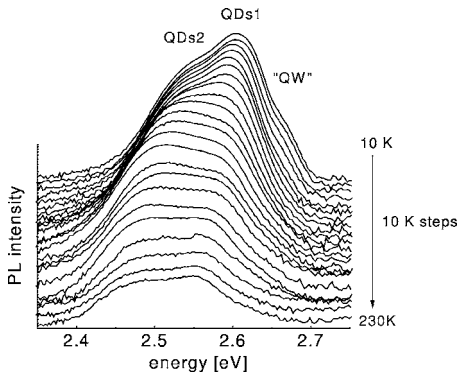

FIG. 3. Temperature dependent PL spectra using 100 fs pulses at 2.85 eV and average intensity of 0.08 W cm^{-2}. The temperature ranges from 10 K to 230 K in 10 K steps as labeled. QDs1 and QDs2 denote high and low energy quantum dots, respectively, symbol QW denotes quantum-well-like QD precursors of CdSe.

and 180 K the QDs2 peak exceeds the height of the QDs1 peak. At temperatures above 180 K the QDs1 band again gains importance and finally exceeds the intensity of the low energy QDs2 band.

The observed temperature behavior gives, first of all, additional strong experimental evidence for the presence of two spectrally resolvable QD distributions in the studied sample, whose emission can be followed up to very high temperatures. Furthermore, the changes in relative intensity between these two bands indicate a coupled thermalization of carriers between the QD distributions. Qualitatively, the rapid decrease of the QDs1 emission at lower temperatures is explained by thermally activated nonradiative decay as well as by thermal activation of of QDs1 excitons into the QW precursor states and subsequent trapping by adjacent dots of the QDs2 subset.

The temperature dependent PL spectra were deconvoluted into two Gaussian line shapes each representing one subset of CdSe QDs. In this way the temperature dependence of (a) the integrated PL intensities, (b) the peak photon energies and (c) the full widths at half maximum (FWHM) of the emission bands were obtained. In Fig. 4 we plot the integrated intensity extracted from both PL bands. The high-

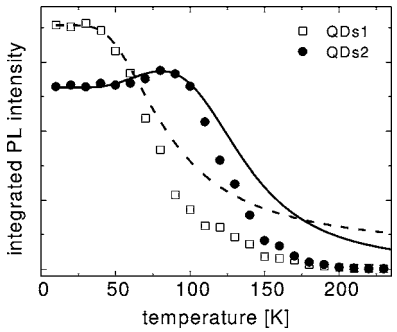

FIG. 4. Extracted integrated PL intensity of the Gaussian QDs1 and QDs2 emission bands as a function of temperature. The full and dashed line are model calculations as described in the text using the decay times given in Table I and localization energies Δ_1=23 meV and Δ_2=65 meV.

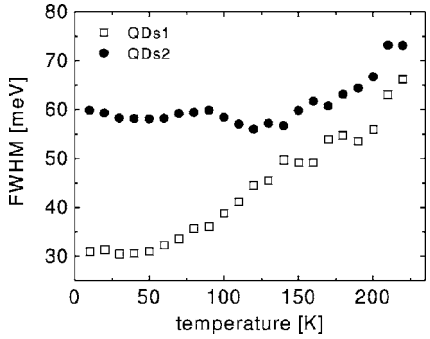

FIG. 5. Full width at half maximum (FWHM) of the Gaussian QDs1 and QDs2 emission bands as a function of temperature.

energy QDs1 intensity substantially decreases with increasing temperature while the QDs2 intensity increases with a maximum intensity observed at ~80 K followed by a PL intensity decrease above 100 K. To a first approximation, the observed integrated PL intensity is proportional to the number of excited QD excitons that recombine radiatively. As the temperature increases, the interplay of capture, thermal activation and recombination between the two QD distributions becomes important.

The FWHM values of both QD emission bands vary slightly for temperatures between 10 and 60 K as shown in Fig. 5. At higher temperature the FWHM of the QDs1 emission increases from 30 meV to 70 meV which is attributed to a thermally induced redistribution of carriers within the QDs1 subensemble from stronger localized into less localized states and into CdSe QW precursor states located on the high energy side of the QDs1 band. In contrast, the FWHM of the low energy QDs2 band remains nearly constant (~60 meV up to 150 K) which is attributed to the strong localization energy of QDs2 that prevents a thermally induced redistribution of carriers within the QDs2 subset. Above 150 K the FWHM of the QDs2 band also starts to broaden due to the onset of thermal redistribution.

We observe that the peak energy positions presented in Fig. 6 monotonically decrease with increasing temperature. In accordance to the weak thermal redistribution of QDs2 excitons the red shift of the strongly localized QDs2 emission is mainly attributed to the reduction of the band-gap energy with increasing temperature. The weaker energy shift of the QDs1 band is explained by the thermally activated

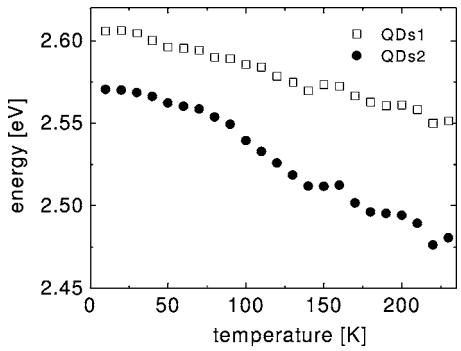

FIG. 6. Extracted maximum energy position of the Gaussian QDs1 and QDs2 emission bands as a function of temperature.

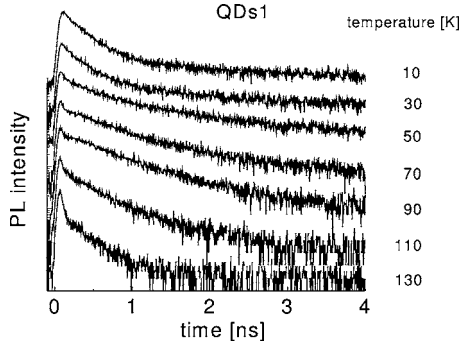

FIG. 7. Time-resolved PL traces on a logarithmic scale recorded at the maximum position of the Gaussian QDs1 emission at different temperatures as labeled. The sample was excited with 100 fs pulses at 3.08 eV. For a better comparison the traces are offset to each other.

transfer of excitons from stronger into weaker localized QDs1 states. This carrier redistribution shifts the center QDs1 emission to higher energy thus counteracting the band-gap energy reduction which results in a weaker "effective" redshift with increasing temperature for this QD subset.

The dynamics of excitons in the bimodal QD distribution has been investigated by spectrally resolved transient PL measurements. Figures 7 and 8 depict the PL decay traces between 10 and 130 K at the maximum position of the Gaussian QDs1 and QDs2 emission, respectively. For a better comparison the traces are offset to each other. In both QDs subsets we find a rapidly decaying component shortly (~0.1 ns) after the arrival of the excitation pulse. Due to its short emission time its contribution to the total time integrated PL intensity is low but increases with increasing temperature. We attribute this rapid PL peak to the emission of QDs with defective crystalline environment that contains dislocations and hence have a high nonradiative recombination rate. We believe that these defective QDs are preferably located close to dislocations found in plane view TEM investigations of this sample.

Besides this striking PL spark the time traces exhibit a nonexponential decay at low temperatures (10–50 K) that is typical for a nonuniform QD distribution [18,21,58,59]. Up to

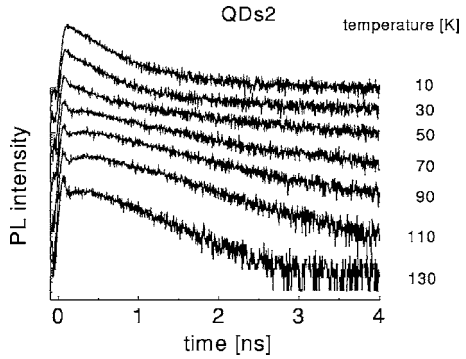

FIG. 8. Time-resolved PL traces on a logarithmic scale recorded at the maximum position of the Gaussian QDs2 emission at different temperatures as labeled. For a better comparison the traces are offset to each other.

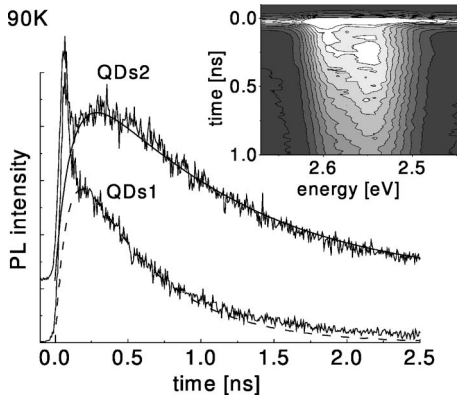

FIG. 9. Time-resolved PL traces recorded at the maximum position of the QDs1 and QDs2 emission at 90 K. The full and dashed line are model calculations as described in the text. The inset shows a contour plot of the time resolved PL spectrum.

50 K the PL trace reveals a decrease of the decay rate with increasing temperature for both subsets. This behavior is explained by a thermally activated population of bright-exciton states from energetically lower dark-exciton states due to phonon-assisted spin relaxation with a relaxation time of typically ~10 ns.[60,61] This bright-exciton repopulation leads to a prolonged effective lifetime as observed and as described in other QD systems.[61] Above 50 K the PL of QDs1 shows a weak signal rise with peak around ~0.2 ns and then decreases due to thermal population of excited exciton states and thermally activated escape into CdZnSSe QD-precursor states and into nonradiative centers. As expected the decay rate increases with increasing temperature. The exciton dynamics of the QDs2 ensemble shows a more pronounced signal rise as the QDs1 PL which peaks at ~0.25 ns before it decays at longer times. The PL decay of QDs2 excitons that increases with increasing temperature is explained as for the QDs1 subset.

The exciton dynamics at the maximum position of the QDs1 and QDs2 emission is again displayed in Fig. 9 at 90 K on a linear scale. Also shown is the time resolved spectrum as a contour plot in the inset. The graphs clearly show the pronounced initial peak, the signal rise for both QDs subsets and the subsequent decay due to thermally activated escape and nonradiative recombination of the QD excitons.

IV. MODEL DESCRIPTION AND DISCUSSION

To model the observed complex QD relaxation dynamics we introduce the following simplifying approximations: We neglect the contribution of imperfect QDs which cause the initial PL spark assuming that these QDs are concentrated at the barrier-wetting layer interface so that their presence does not significantly affect the dynamics of intact QDs. We further neglect any dark-states to bright-states dynamics. We assume two sets of uniform QDs (1 and 2) with different exciton confinement (localization) energies Δ_1 and Δ_2 that are embedded within wetting layer QW. We assume a temperature independent radiative decay rate γ_{radw} of wetting layer excitons and a capture rate γ_w of QW excitons captured by QDs1 and QDs2. No nonradiative decay of QW excitons is taken into account. Furthermore we assume temperature independent radiative decay rates $\gamma_{rad1(2)}$ and nonradiative decay rates $\gamma_{nrad1(2)}$ of excitons in QDs1 and QDs2, respectively. Since the repetition time in our time integrated (12.5 ns) and time-resolved measurements (4 μs) is longer than the QD decay time (~2–4 ns) the rate equations for excitons at low excitation densities (neglecting saturation effects) can be given as

$$\frac{\partial n_w}{\partial t} = -n_w\gamma_{radw} - n_w\gamma_w + n_1\gamma_w \exp\left(-\frac{\Delta_1}{k_BT}\right) + n_2\gamma_w \exp\left(-\frac{\Delta_2}{k_BT}\right), \quad (1)$$

$$\frac{\partial n_1}{\partial t} = -n_1\gamma_{rad1} + n_w\gamma_w C_1 - n_1\gamma_w \exp\left(-\frac{\Delta_1}{k_BT}\right) - n_1\gamma_{nrad1} \exp\left(-\frac{\Delta_1}{k_BT}\right), \quad (2)$$

$$\frac{\partial n_2}{\partial t} = -n_2\gamma_{rad2} + n_w\gamma_w C_2 - n_2\gamma_w \exp\left(-\frac{\Delta_2}{k_BT}\right) - n_2\gamma_{nrad2} \exp\left(-\frac{\Delta_2}{k_BT}\right). \quad (3)$$

Here subscripts w, 1, and 2, denote the wetting layer as well as QDs1 and QDs2, n_w, n_1, and n_2 are the number of excitons in QW, in QDs1 and in QDs2, respectively. k_B is the Boltzmann constant. Constants $C_1 = n_{QDs1}/n_{QD}$ and $C_2 = n_{QDs2}/n_{QD}$ give the ratios of the QDs1(2) density relative to the total quantum dot density n_{QD}. The model couples the two QD subsets via thermal escape of QD excitons with rate γ_w. It further proposes thermally activated nonradiative decay with different rates $\gamma_{nrad1(2)}$ for the two QD subsets.

At low temperatures thermally activated coupling as well as nonradiative decay can be neglected. The PL decay from the two different QD exciton distributions is approximately given by $n_{ph1(2)}(t) \propto \exp(-\gamma_{rad1(2)}t)$ where $\gamma_{rad1(2)}$ are the radiative decay rates of QDs1 and QDs2. As mentioned already the "effective" radiative decay rate due to dark-state filling decreases with increasing temperature from $\gamma_{rad1(2)} \approx 2.5\times10^9$ s^{-1} at 10 K to $\gamma_{rad1(2)} \approx 1\times10^9$ s^{-1} at 50 K for both subsets. Above 50 K the nonradiative rates $\gamma_{nrad1(2)}$ and escape rate γ_w were determined by fitting the solutions of Eqs. (1)–(3) with the PL traces. For the numerical calculations we use the effective radiative rate of $\gamma_{rad1(2)} = 1\times10^9$ s^{-1} obtained at 50 K. Since we only observe a very weak QW luminescence at low temperatures we conclude that $\gamma_{radw} \ll \gamma_w$. The localization energies $\Delta_1 \approx 25$ meV and $\Delta_2 \approx 65$ meV are estimated from the energetic difference of the PL peak energies to the wetting layer emission QW at 10 K (see Fig. 3). Best agreement between experimental and numerical traces in the range 70 and 130 K was found for parameters $\gamma_w = 0.9\times10^{10}$ s^{-1}, $\gamma_{nrad1} = 1.4\times10^{10}$ s^{-1}, and $\gamma_{nrad2} = 2.5\times10^{11}$ s^{-1}. Figure 9 compares the traces of experimental and numerical traces of the QDs1 (dashed line)

TABLE I. Decay rates used to simulate the dynamical behavior of the bimodal QD distribution. γ_{rad1} and γ_{rad2} are the radiative decay rates, γ_{nrad1} and γ_{nrad2} denote nonradiative decay rates, of QDs1 and QDs2, respectively. γ_w is the capture rate from QW states.

$\gamma_{rad1(2)}$	1×10^{9} s^{-1}
γ_{nrad1}	1.4×10^{10} s^{-1}
γ_{nrad2}	2.5×10^{11} s^{-1}
γ_w	0.9×10^{10} s^{-1}

and QDs2 (full line) emission at 90 K. The agreement between experimentally observed PL and model calculations is comparably good for the other temperatures.

The numerical analysis reveals a striking difference between nonradiative rates γ_{nrad2} and γ_{nrad1} by more than one order of magnitude. As possible explanation we propose a different coupling to nonradiative recombination centers for the two QD subsets due to different QD accumulations at defects. In particular the strong confinement of QDs2 indicates a higher Cd concentration as compared to QDs1. Therefore QDs2 are preferably expected in Cd-rich QD-precursor areas. As already mentioned plane-view TEM investigations reveal defects with a density of 8×10^{8} cm^{-2} that are supposed to originate at highly strained CdSe-rich regions. We therefore conclude that QDs2 are most likely located adjacent to these defects leading to a high nonradiative rate for this type of QDs.

Using the extracted decay rates that are summarized in Table I we calculated the time integrated photon emission that are emitted from QDs1 and QDs2 according to

$$n_{ph1(2)}(T) = \int_0^\infty \gamma_{rad1(2)} n_{1(2)}(t,T)dt. \tag{4}$$

Photon numbers $n_{ph1}(T)$ and $n_{ph2}(T)$ are proportional to the observed integrated intensity of the stationary PL emission obtained from the bimodal QD distribution at given temperature T. In Fig. 4 the calculated time integrated PL intensities shown as dashed (QDs1) and full lines (QDs2) are compared with experimentally obtained PL.

Despite the limitations and approximations of the proposed model the calculated curves are in fair agreement with the experimental data. In particular the increasing QDs2 emission with maximum at about 80 K is nicely reproduced. However, the calculations show significantly higher PL intensities for temperatures above 100 K for both QD subsets. This deviation is mainly attributed to the simplifying assumption that the number of barrier excitons that reach the wetting layer (n_w) remains constant with increasing temperature. Thermal activation may induce nonradiative recombination within the barrier and in the wetting layer (e.g., by reactivation of wetting layer excitons back into the barrier or into barrier or wetting layer interface states) thus reducing the number of excitons that finally can be trapped by the QDs. This explanation is further supported by the reduction of the PL spark intensity observed in the time-resolved measurements when the temperature is increased from 10 to 130 K.

V. SUMMARY

We have investigated the dynamical behavior of a bimodal distribution of QD excitons by intensity and temperature dependent time-integrated and time-resolved PL. At low intensities we observe a dominant exciton emission from QDs1 with weak localization and a weaker emission from QDs2 with higher localization. At high excitation densities the emission of quantum-well-like CdSe QD-precursor states QW become visible on the high energy side of QDs1. In addition the peak position of the QDs1 and QDs2 band shifts to lower energies at high excitation levels which is attributed to increased exciton scattering and to the formation of biexcitons and negatively charged excitons. The thermal dependence of the integrated QDs1 and QDs2 PL intensity indicates a thermally activated population of QDs2 with excitons that escaped from QDs1. Time resolved PL measurements enabled us to estimate the characteristic radiative and nonradiative decay rates as well as exciton escape rates so as to simulate the observed behavior using a simplified coupled rate equation model. Within the model limitations the experimental data is reasonably reproduced. Deviations from the experimental observations obtained above 100 K are mainly attributed to the neglect of nonradiative recombination of barrier and QW excitons in our model.

ACKNOWLEDGMENTS

Two authors (M.S. and S.M.) were supported by the Alexander von Humboldt Foundation. Plan-view TEM investigations by I. Haeusler, Humboldt University Berlin, and experimental support of H. Schmitzer, Xavier University, and of H.-P. Tranitz are kindly acknowledged. This work is supported by the National Science Foundation (Grant No. DMR 0305076).

*Present address: Department of Chemistry and Biochemistry, Ludwig-Maximilian-University, Munich, Germany.

[1] M. A. Haase, J. Qiu, J. M. DePuydt, and H. Cheng, Appl. Phys. Lett. **59**, 1272 (1991).

[2] Y. Arakawa and H. Sakaki, Appl. Phys. Lett. **40**, 939 (1982).

[3] For a review see: D. Bimberg, M. Grundmann, and N. N. Ledentsov, *Quantum Dot Heterostructures* (Wiley & Sons, New York, 1999).

[4] H. Sakaki, Surf. Sci. **267**, 623 (1992).

[5] E. L. Ivchenko, A. V. Kavokin, V. P. Kochereshko, P. S. Kopev, and N. N. Ledentsov, Superlattices Microstruct. **12**, 317 (1992).

[6] P. G. Eliseev, H. Li, A. Stintz, G. T. Liu, T. C. Newell, K. J.

Malloy, and L. F. Lester, Appl. Phys. Lett. **77**, 262 (2000).
[7] C. W. Snyder, B. G. Orr, D. Kessler, and L. M. Sander, Phys. Rev. Lett. **66**, 3032 (1991).
[8] Y. C. Zhang, C. J. Huang, F. Q. Liu, B. Xu, J. Wu, Y. H. Chen, D. Ding, W. H. Jiang, X. L. Xe, and Z. G. Wang, J. Appl. Phys. **90**, 1973 (2001).
[9] M. Colocci, A. Vinattieri, L. Lippi, F. Bogani, M. Rosa-Clot, S. Taddei, A. Bosacchi, S. Franchi, and P. Frigeri, Appl. Phys. Lett. **74**, 564 (1999).
[10] Martin Strassburg, O. Schulz, Matthias Strassburg, U. W. Pohl, R. Heitz, A. Hoffmann, D. Bimberg, M. Klude, D. Hommel, K. Lischka, and D. Schikora, Adv. Solid State Phys. **42**, 27 (2002).
[11] D. Schikora, S. Schwedhelm, D. J. As, K. Lischka, D. Litvinov, A. Rosenauer, D. Gerthsen, M. Strassburg, A. Hoffmann, and D. Bimberg, Appl. Phys. Lett. **76**, 418 (2000).
[12] N. Peranio, A. Rosenauer, D. Gerthsen, S. V. Sorokin, I. V. Sedova, and S. V. Ivanov, Phys. Rev. B **61**, 16015 (2000).
[13] R. Engelhardt, U. W. Pohl, D. Bimberg, D. Litvinov, A. Rosenauer, and D. Gerthsen, J. Appl. Phys. **86**, 5578 (1999).
[14] C. Gourdon and P. Lavallard, Phys. Status Solidi B **153**, 641 (1989).
[15] L. E. Golub, S. V. Ivanov, E. L. Ivchenko, T. V. Shubina, A. A. Toropov, J. P. Bergman, G. R. Pozina, B. Monemar, and M. Wilander, Phys. Status Solidi B **205**, 203 (1998).
[16] A. Klochikhin, A. Reznitsky, S. Permogorov, T. Breitkopf, M. Grün, M. Hetterich, C. Klingshirn, V. Lyssenko, W. Langbein, and J. M. Hvam, Phys. Rev. B **59**, 12947 (1999).
[17] S. Yamaguchi, H. Kurusu, Y. Kawakami, S. Fujita, and S. Fujita, Phys. Rev. B **61**, 10303 (2000).
[18] M. Strassburg, M. Dworzak, H. Born, R. Heitz, A. Hoffmann, M. Bartels, K. Lischka, D. Schikora, and J. Christen, Appl. Phys. Lett. **80**, 473 (2002).
[19] S. Nagahama, T. Kozaki, T. Yanamoto, and T. Mukai, Oyo Butsuri **73**, 210 (2004).
[20] T. Suski, H. Teiseyre, S. P. Lepowski, P. Perlin, H. Mariette, T. Kitamura, Y. Ishida, H. Okumura, and S. F. Chichibu, Phys. Status Solidi B **235**, 225 (2003).
[21] S. Rodt, V. Türck, R. Heitz, F. Guffarth, R. Engelhardt, U. W. Pohl, M. Straßburg, M. Dworzak, A. Hoffmann, and D. Bimberg, Phys. Rev. B **67**, 235327 (2003).
[22] Th. Förster, Ann. Phys. **2**, 55 (1948).
[23] A. Reznetsky, A. Klochikhin, and S. Permogorov, Phys. Solid State **39**, 1035 (1997).
[24] A. M. Kapitonov, U. Woggon, K. Leonardi, D. Hommel, K. Edamatsu, and T. Itoh, Phys. Status Solidi C **4**, 317 (2003).
[25] T. Inoshita and H. Sakaki, Phys. Rev. B **46**, 7260 (1992); **56**, R4355 (1997).
[26] N. N. Ledentsov, V. A. Shchukin, M. Grundmann, N. Kirstaedter, J. Böhrer, O. Schmidt, D. Bimberg, V. M. Ustinov, A. Yu. Egorov, A. E. Zhukov, P. S. Kop'ev, S. V. Zaitsev, N. Yu. Gordeev, Zh. I. Alferov, A. I. Borovkov, A. O. Kosogov, S. S. Ruvimov, P. Werner, U. Gösele, and J. Heydenreich, Phys. Rev. B **54**, 8743 (1996).
[27] G. S. Solomon, J. A. Trezza, A. F. Marshall, and J. S. Harris, Phys. Rev. Lett. **76**, 952 (1996).
[28] R. Heitz, I. Mukhametzhanov, P. Chen, and A. Madhukar, Phys. Rev. B **58**, R10151 (1998).
[29] D. L. Huffaker and D. G. Deppe, Appl. Phys. Lett. **73**, 366 (1998).
[30] C. Lobo, R. Leon, S. Marcinkevicius, W. Yang, P. C. Sercel, X. Z. Liao, J. Zou, and D. J. H. Cockayne, Phys. Rev. B **60**, 16647 (1999).
[31] A. Tackeuchi, T. Kuroda, K. Mase, Y. Nakata, and N. Yokoyama, Phys. Rev. B **62**, 1568 (2000).
[32] U. Jahn, M. Ramsteiner, R. Hey, H. T. Grahn, E. Runge, and R. Zimmermann, Phys. Rev. B **56**, R4387 (1997).
[33] M. Grassi Alessi, F. Fragano, A. Patanè, M. Capizzi, E. Runge, and R. Zimmermann, Phys. Rev. B **61**, 10985 (2000).
[34] R. Zimmermann and E. Runge, Phys. Rev. B **69**, 155307 (2004).
[35] A. Klochikhin, A. Reznitsky, B. Dal Don, H. Priller, H. Kalt, C. Klingshirn, S. Permogorov, and S. Ivanov, Phys. Rev. B **69**, 085308 (2004).
[36] U. W. Pohl, R. Engelhardt, V. Türck, and D. Bimberg, J. Cryst. Growth **195**, 569 (1998).
[37] V. Türck, S. Rodt, O. Stier, R. Heitz, R. Engelhardt, U. W. Pohl, D. Bimberg, and R. Steingrüber, Phys. Rev. B **61**, 9944 (2000).
[38] F. Gindele, U. Woggon, W. Langbein, J. M. Hvam, K. Leonardi, D. Hommel, and H. Selke, Phys. Rev. B **60**, 8773 (1999).
[39] J. Puls, M. Rabe, and F. Henneberger, J. Cryst. Growth **214**, 774 (2000).
[40] J. Seufert, R. Weigand, G. Bacher, T. Kümmell, A. Forchel, K. Leonardi, and D. Hommel, Appl. Phys. Lett. **76**, 1872 (2000).
[41] S. H. Xin, P. D. Wang, Aie Yin, M. Dobrowolska, J. L. Merz, and J. K. Furdyna, Appl. Phys. Lett. **69**, 3884 (1996).
[42] F. Flack, N. Samarth, V. Nikitin, P. A. Crowell, J. Shi, J. Levy, and D. D. Awschalom, Phys. Rev. B **54**, R17312 (1996).
[43] M. Strassburg, V. Kutzer, U. W. Pohl, A. Hoffmann, I. Broser, N. N. Ledentsov, D. Bimberg, A. Rosenauer, U. Fischer, D. Gerthsen, I. L. Krestnikov, M. V. Maximov, P. S. Kop'ev, and Zh. I. Alferov, Appl. Phys. Lett. **72**, 942 (1998).
[44] K. Leonardi, H. Heinke, K. Ohkawa, and D. Hommel, Appl. Phys. Lett. **71**, 1510 (1997).
[45] S. Sanguinetti, M. Henini, M. Grassi Alessi, M. Capizzi, P. Frigeri, and S. Franchi, Phys. Rev. B **60**, 8276 (1999).
[46] J. W. Tomm, T. Elsaesser, Yu I. Mazur, H. Kissel, G. G. Tarasov, Z. Ya. Zhuchenko, and W. T. Masselink, Phys. Rev. B **67**, 045326 (2003).
[47] W. Yang, R. R. Lowe-Webb, H. Lee, and P. C. Sercel, Phys. Rev. B **56**, 13314 (1997).
[48] S. Mackowski, G. Prechtl, W. Heiss, F. V. Kyrychenko, G. Karczewski, and J. Kossut, Phys. Rev. B **69**, 205325 (2004).
[49] Yu. I. Mazur, J. W. Tomm, G. G. Tarasov, H. Kissel, C. Walther, Z. Ya. Zhuchenko, and W. T. Masselink, Physica E (Amsterdam) **13**, 255 (2002).
[50] L. Brusaferri, S. Sanguinetti, E. Grill, M. Guzzi, A. Bignazzi, F. Bogani, L. Carraresi, M. Colocci, A. Bosacchi, P. Frigere, and S. Franchi, Appl. Phys. Lett. **69**, 3354 (1996).
[51] Y. C. Zhang, C. J. Huang, F. Q. Liu, B. Xu, J. Wu, Y. H. Chen, D. Ding, W. H. Jiang, X. L. Ye, and Z. G. Wang, J. Appl. Phys. **90**, 1973 (2001).
[52] M. Strassburg, Th. Deniozou, A. Hoffmann, R. Heitz, U. W. Pohl, D. Bimberg, D. Litvinov, A. Rosenauer, D. Gerthsen, S. Schwedhelm, K. Lischka, and D. Schikora, Appl. Phys. Lett. **76**, 685 (2000).
[53] M. Straßburg, J. Christen, M. Dworzak, R. Heitz, A. Hoffmann, M. Bartels, K. Lischka, and D. Schikora, Phys. Status Solidi B **229**, 529 (2002); M. Strassburg, M. Dworzak, R. Heitz, A. Hoffmann, J. Christen, and D. Schikora, Mater. Sci. Eng., B **88**, 302 (2002).
[54] H.-P. Tranitz, H. P. Wagner, R. Engelhardt, U. W. Pohl, and D.

Bimberg, Phys. Rev. B **65**, 035325 (2002).
[55] T. Kümmell, R. Weigand, G. Bacher, A. Forchel, K. Leonardi, D. Hommel, and H. Selke, Appl. Phys. Lett. **73**, 3105 (1998).
[56] G. Bacher, R. Weigand, J. Seufert, V. D. Kulakovskii, N. A. Gippius, A. Forchel, K. Leonardi, and D. Hommel, Phys. Rev. Lett. **83**, 4417 (1999).
[57] M. Strassburg, R. Heitz, V. Türck, S. Rodt, U. W. Pohl, A. Hoffmann, D. Bimberg, I. L. Krestnikov, V. A. Shchukin, N. N. Ledentsov, Zh. I. Alferov, D. Litvinov, A. Rosenauer, and D. Gerthsen, J. Electron. Mater. **28**, 506 (1999).
[58] T. Okuno, H.-W. Ren, M. Sugisaki, K. Nishi, S. Sugou, and Y. Masumoto, Phys. Rev. B **57**, 1386 (1998).
[59] S. Lee, J. C. Kim, H. Rho, C. S. Kim, L. M. Smith, H. E. Jackson, J. K. Furdyna, and M. Dobrowolska, Phys. Rev. B **61**, R2405 (2000).
[60] T. Flissikowski, A. Hundt, M. Lowisch, M. Rabe, and F. Henneberger, Phys. Rev. Lett. **86**, 3172 (2001).
[61] B. Patton, W. Langbein, and U. Woggon, Phys. Rev. B **68**, 125316 (2003).